The onset of Neoglaciation 6000 years ago in western Mongolia revealed by an ice core from Tsambagarav mountain range

Pierre-Alain Herren[1,2], Anja Eichler[1,2], Horst Machguth[3,4], Tatyana Papina[5], Leonhard Tobler[1,2], Alexander Zapf[1,2] and Margit Schwikowski[1,2,6]

[1]Paul Scherrer Institut, 5232 Villigen PSI, Switzerland

[2]Oeschger Centre for Climate Change Research, University of Bern, 3012 Bern, Switzerland

[3]Glaciology and Geomorphodynamics, University of Zürich, 8057 Zürich, Switzerland

[4]Geological Survey of Denmark and Greenland, 1350 Copenhagen, Denmark

[5]Institute for Water and Environmental Problems, 656038 Barnaul, Russia

[6]Department of Chemistry and Biochemistry, University of Bern, 3012 Bern, Switzerland

Corresponding author: Margit Schwikowski

E-mail: margit.schwikowski@psi.ch, Phone: +41 56 310 4110

Address: Paul Scherrer Institut, 5232 Villigen PSI, Switzerland

Abstract

Glacier highstands since the Last Glacial Maximum are well documented for many regions but little is known about glacier fluctuations and lowstands during the Holocene. This is because the traces of minimum extents are difficult to identify and at many places are still ice covered, limiting the access to sample material. Here we report a new approach to assess minimal glacier extent, using a 72 meter long surface-to-bedrock ice core drilled on Khukh Nuru Uul, a glacier in the Tsambagarav mountain range of the Mongolian Altai (4130 m asl, 48°39.338'N, 90°50.826'E). The small ice cap has low ice temperatures and flat bedrock topography at the drill site which is ideal for a climate archive. The upper two-thirds of the ice core contain 200 years of climate information with annual resolution, whereas the lower third is subject to strong thinning of the annual layers with a basal ice age of approximately 6000 years before present (BP). We interpret the basal ice age as indicative of ice-free conditions in the Tsambagarav mountain range at 4100 m asl prior to 6000 years BP. This age marks the onset of the Neoglaciation at the end of the Holocene Climate Optimum. The ice-free conditions allow for adjusting the Equilibrium Line Altitude (ELA) and derive the glacier extent in the Mongolian Altai during the Holocene Climate Optimum. Based on the ELA-shift we conclude that most of the glaciers are not remnants of the Last Glacial Maximum but were formed during the second part of the Holocene. The ice core derived accumulation reconstruction suggests important changes in the precipitation pattern over the last 6000 years. During formation of the glacier wetter conditions than presently prevailed, followed by a long dry period from 5000 years BP until 250 years ago.

Present conditions are wetter than during the past millennia. This is consistent with precipitation evolution derived from lake sediment studies in the Altai.

Keywords

Ice core, radiocarbon, Holocene, Neoglaciation, climate, Mongolian Altai

1. Introduction

The Holocene can be divided in three phases; the early deglaciation period (11,600 to 9000 years BP), the Holocene Climate Optimum (HCO, 9000 to 5000-6000 years BP) and the Neoglaciation period (5000-6000 years BP to preindustrial time). Discussions about amplitude, duration, and causes of the different phases initiated numerous studies and generated new paleoclimatic records. The hypothesis of a relative stable Holocene climate [*Johnsen et al.*, 1997] compared to glacial interglacial changes has been contested and recurring cold events (so called "Bond cycles") with a periodicity of 1470±500 years have been proposed for the Holocene [*Bond et al.*, 1997; *Mayewski et al.*, 2004]. However, *Wanner et al.* [2011] did not observe periodic cold relapses during the last 10 kyr and contradicts the occurrence of "Bond cycles" for the Holocene. Additionally the current debate about anthropogenic climate change raises the question if during the past 10 kyr temperatures higher or similar than today may have occurred. Generation and analysis of proxy data covering the Holocene epoch is thus of major importance in order to better understand the current climate change. In this context glacier fluctuations can be used to study trends of temperature and precipitation during the Holocene [*Oerlemans*, 2005; *Solomina et al.*, 2008; *Davis et al.*, 2009; *Owen*, 2009]. Most approaches rely on distinctive features such as terminal moraines or exposure dating to reconstruct maximum glacier extents. The current retreat of glaciers provides a unique opportunity to collect ancient embedded organic particles [*Miller et al.*, 2012], wood fragments [*Ivy-Ochs et al.*, 2009], or archeological remnants [*Grosjean et al.*, 2007; *Nesje et al.*, 2012]. Artifacts exposed at the front of the glacier tongues are dated and allow for reconstructing glacier fluctuation chronologies.

However, for inferring minimum extent of glaciers such specific features are difficult to identify and the access to potential sample material is often hindered by ice coverage. Consequently little is known about glacier lowstands and the discussion is ongoing which high-mountain glaciers and ice caps have persisted throughout the Holocene and which have disappeared at some point. A promising approach to overcome the lack of evidence is the use of high-resolution ice core records extracted from alpine glaciers. They may provide insight in former climate conditions [e.g. *Thompson et al.*, 1998; *Eichler et al.*, 2011] and may give access to datable material in the basal ice itself or from the bedrock.

The Intergovernmental Panel on Climate Change (IPCC) projection of total disappearance of Himalayan glaciers by 2035, a statement finally recalled, had the merit to increase the public awareness about glacier changes in Asia, their importance, and impacts on society. Most investigations dealing with Asian quaternary glacier fluctuations have focused on the Himalaya and the Tibetan Plateau [*Lehmkuhl and Owen*, 2005; *Davis et al.*, 2009], likewise the ice core drilling projects. The adjacent mountain ranges including the Pamir, Tien Shan, and Altai have received less attention and were thereby investigated in less detail. For a complete understanding of glacier fluctuations in Asia, more research in these regions is required. Here we date an ice core from the Altai Mountains to examine glacier behavior and reconstruct accumulation rates during the Holocene.

2 Regional setting

The Altai Mountains, a complex mountain system in Central Asia, form the borders between Russia, Kazakhstan, China, and Mongolia. The maximum elevation is 4500 m asl and the range extends over approximately 1200 km [*Rudaya et al.*, 2009]. According to the Randolph Glacier Inventory (RGI, [*Arendt et al.* 2012]) and Landsat imagery used to manually correct the RGI, data the Altai has a glaciated area of roughly 1300 km^2 including approximately 500 km^2 of Mongolian glaciers. From northwest (Russian Altai) to southeast (Mongolian Altai) where the foothills reach the Gobi desert, the mountain range serves as watershed between the Arctic Ocean and the basin of central Asia. The location and extent imply a major role in the Asian climate system and thus, requires thorough paleoclimate investigations, all the more since instrumental data is limited and spatially sparse.

The mountain chain acts like a barrier and intercepts air masses originating from the west, leading to a strong northwest to southeast precipitation gradient. In the Russian Altai yearly precipitation is around 800 mm and decreases to less than 200 mm in the floor of the intermountain depressions of the Mongolian Altai [*Klinge et al.*, 2003]. The Siberian High controls the winter climate with cold and dry conditions. Most of the precipitation is related to the Westerlies and occurs mainly during the months June, July, and August [*Klinge et al.*, 2003].

Glacier fluctuation studies dealing with the Altai mountain range are mainly limited to the late Pleistocene [*Lehmkuhl et al.*, 2011], whereas knowledge for the Holocene period is rare. A detailed discussion of glacier fluctuations from *Agatova et al.* [2012] refutes the former general concept of a gradual retreat of

121 the Würm glaciers in the Russian Altai by summarizing former work and
122 presenting new data. For the period 7000 years BP to present temperature and
123 humidity reconstructions are presented based on lichenometry,
124 geomorphological methods, and further radiocarbon dates from formerly buried
125 wood pieces. Forest regrowth in presently glaciated areas during interstage
126 warm periods suggest strong glacier retreat or even complete disappearance
127 especially during the HCO. Additionally the recovery of wood fragments
128 originating from the HCO above the modern tree line indicates warmer
129 temperatures than nowadays. After a glacier-hostile climate glaciers started to
130 regrow around 5000 years BP. Periods of glacier advances (8300, 5700, 4000,
131 and 400 years BP) have been proposed for western China [*Zhou et al.*, 1991]
132 adjacent to the Mongolian Altai. Glacier advances detected around 5700 years BP
133 in western China, occured slightly earlier than in the Russian Altai and can be
134 interpreted as the end of the HCO and the onset of the Neoglaciation.
135 Lake sediment cores collected in Hoton-Nur lake (northwestern Mongolia, Figure
136 1) show distinct variations in the precipitation. A major shift from wet to present
137 dry conditions occurred 5000 years BP [*Rudaya et al.*, 2009; *Mackay et al.*, 2012].
138 Information about glacier fluctuations and past temperature is not available.
139 Long-term Holocene climate records for the Mongolian Altai are thus incomplete
140 and biased towards lake sediment data.
141 For the Mongolian Altai high-resolution climate reconstructions on a millennial
142 scale are based on tree-ring chronologies. Most studies provide records for few
143 centuries only, the longest currently available covers 1700 years [*D'Arrigo et al.*,
144 2001; *Loader et al.*, 2010]. The reconstruction suggests that the coldest and
145 warmest conditions of the last millennia occurred during the 19th and 20th

century. Further back in time the different records show less coherent behavior and thus require more data for accurate past climate information. The only alternative reconstructions originate from an ice core drilled in the Russian Altai spanning 750 years [*Eichler et al.*, 2009a; 2009b]. For the Siberian Altai a correlation between solar forcing and temperature was found for the period 1250 to 1850 AD. Additionally the biogenic emissions from the Siberian forests are closely related to temperature changes. However, no long-term reconstructions of Holocene glacier fluctuations in the Mongolian Altai exist. This work is a step towards an improvement in understanding the climate of Central Asia. We present a multi-proxy approach using an ice core covering approximately the last 6000 years and provide a larger perspective on the Holocene climate in the Mongolian Altai.

3 Experimental Methods

3.1 Ice core drilling

In July 2009 a joint Russian-Swiss expedition collected a 72 m surface-to-bedrock ice core and an adjacent 52 m parallel core in the Tsambagarav mountain range situated in the Mongolian Altai (4140 m asl, 48°39.338'N, 90°50.826'E). This mountain range is dominated by small ice caps, with the ice margin varying between 3000 and 3800 m asl (Figure 1) strongly depending on the exposition. The total area of glaciation was 73.2 km^2 by 2008 [*Demberel*, 2011]. The equilibrium line altitude (ELA) is estimated to be at 3700 m asl [*Lehmkuhl et al.*, 2011]. Prior to the expedition the drill site was selected based on satellite imagery (Landsat 7 / 8.8.2002 / http://landsat.usgs.gov/index.php) and the Shuttle Radar Topography Mission Digital Elevation Model (SRTM DEM,

90 m horizontal resolution). The mountain massive is dominated by two peaks of similar elevation: Tsast Uul (4190 m asl) and Khukh Nuru Uul (4130 m asl, elevations derived from SRTM DEM). While the glaciation of Tsast Uul is larger by area, the ice cap appeared less suitable for drilling because of being strongly asymmetric with a steep ice face directly north of the summit. Although slightly lower, Khukh Nuru Uul was chosen because of its rather symmetric ice cap, which promised ideal conditions for undisturbed layering of accumulation.

For drilling the lightweight electromechanical device FELICS [*Ginot et al.*, 2002] was used. Based on previous work by *Schotterer et al.* [1997] and snow accumulation estimations by *Lehmkuhl*, [1998] an ice core covering the last two millennia was expected. Ice segments of 0.7 m in length and 8.25 cm in diameter were packed and sealed on-site in polyethylene bags and transported in frozen condition to Switzerland, where they were processed. Drilling and transportation of the fragile ice cores required major logistical efforts involving helicopter flights from Russia to Mongolia and back, since the region has poor infrastructure, most of the roads are unpaved and freezing facilities are scarce. In the following we use the term Tsambagarav ice core when referring to the ice core from Khukh Nuru Uul glacier.

3.2 Glaciological survey

Ice thickness measurements were performed with radar echo sounding (Malå Ground Penetrating Radar system with 100 and 200 MHz unshielded antennas), combined with a GPS survey. In total 2030 m of radar profiles were measured with roughly half of the profiles located on the summit of Khukh Nuru Uul to construct a detailed map of bed topography around the drill site. Interpretation

196 of the radar signals shows very clear reflections from the bedrock with weak
197 internal reflections from the glacier ice (Figure 2). The undisturbed signal points
198 towards the absence of any liquid water in the glacier ice. Measured two-ways
199 travel time of the radar signal was converted to ice thickness using a velocity of
200 0.175 m ns^{-1}, yielding a glacier thickness of 70.7±0.5m at the drilling site. The
201 detailed array of radar profiles around the drill site shows flat bed topography
202 (Figure 2). The surface and bedrock geometry suggest minimal ice flow implying
203 an undisturbed chronology within the ice core. After drilling a thermistor chain
204 was lowered into the borehole to measure the glacier temperature. Borehole
205 temperatures were cold, ranging from -13.8 to -12.6°C (Figure 3). Thus, the
206 glacier is frozen to bedrock. With such low temperatures, meltwater produced
207 occasionally at the surface during summer months refreezes mainly within the
208 yearly accumulation, creating melt features and preserving the environmental
209 signal stored in the ice. Melt features are bubble free ice lenses with higher
210 density than the surrounding firn [*Henderson et al.*, 2006] thus identifiable in the
211 density profile. Higher summer temperatures during the last decades have led to
212 an aggregation of these melt features within the upper 12 meters, clearly visible
213 in the density profile (Figure 3). To account for increasing density towards
214 bedrock, all depth values are in the following given in meters water equivalents
215 (m weq), where not stated differently. The 72 meter long ice core corresponds to
216 58 m weq.
217
218 *3.3 Analytical methods*
219 Ice core sampling was performed at the cold room of the Paul Scherrer Institut
220 (PSI) at -20°C. Prior to processing, ice core segments were backlit in the

221 darkened cold room to observe dust horizons and ice lenses. A specially designed
222 stainless steel band saw with Teflon coverage on the tabletop was used for
223 sample preparation. For contamination-sensitive species such as major ions (e.g.
224 calcium, formate, ammonium, and sulfate) the inner part of the ice core was used
225 and analyzed by standard ion chromatography techniques. The resolution
226 ranged from 2.5 cm at the top to 2 cm from 50 m depth downwards.
227 For measurements of tritium (^{3}H) and ^{210}Pb the outer part of the ice core was
228 used since those are less sensitive to contamination. Two series of ^{3}H activity
229 measurements were performed by liquid scintillation counting: A first set at low-
230 resolution (60 cm) and a second set at high-resolution (20 cm) for a refined
231 location of the horizon within the ice core [*Eichler et al.*, 2000]. The ^{210}Pb was
232 measured by α-spectroscopy [*Gäggeler et al.*, 1983] with a resolution ranging
233 from 1.0 to 1.4 meters.
234 Ten samples of the lower 20 m weq of the ice core were prepared for ^{14}C analysis
235 of the particulate organic carbon fraction, according to the procedure described
236 in *Jenk et al.* [2009] and *Sigl et al.* [2009]. In comparison to other sites the carbon
237 concentrations at Tsambagarav allowed relative small sample volumes ranging
238 from 143 to 278 ml, resulting in carbon amounts varying between 19 and 58 µg.
239 For decontamination purposes the outer part of the ice core segment was
240 removed with the band saw and the inner part was rinsed with ultra-pure water.
241 To extract the particulate carbon, ice samples were melted, filtered, and acidified
242 with HCl to remove carbonates. A two-step combustion at 340°C and 650°C
243 separates filtered particulate carbon into the organic (OC) and elemental carbon
244 (EC) fraction [*Szidat et al.*, 2004]. The generated CO_2 was cryogenically trapped
245 and sealed in glass tubes for accelerator mass spectrometry (AMS)

measurements. The 200 kV 'MICADAS' AMS system with a gas ion source [*Ruff et al.*, 2007; *Synal et al.*, 2007] allows direct measurements of gas samples. Details about the samples and results are given in Table I.

The ^{14}C values were calibrated using the OxCal software and the IntCal 09 calibration curve [*Ramsey*, 2001; *Reimer et al.*, 2009]. Ages are given in calibrated radiocarbon ages (cal years BP = years before 1950). Dates are given with their 1σ-range.

4 *Dating of the ice core archive for the period 1815-2009 AD*

For obtaining high-resolution climate information based on ice core data the establishment of an age-depth scale is crucial. The dating of the upper 36 m weq was performed using a combination of several methods as described in the following.

4.1 Identification of reference horizons

Thermonuclear bomb tests have accumulated ^{3}H in the atmosphere reaching maximum concentrations in 1963, the year of the partial Test Ban Treaty. Identification of the ^{3}H peak in ice core records served as time marker in many previous investigations [e.g. *Eichler et al.*, 2000; *Knüsel et al.*, 2003; *Olivier et al.*, 2004]. Maximum activity of 6202 ± 62 Tritium Units (TU, decay corrected to the year 1963) is located at a depth of 15.4 m weq (Figure 4) which is comparable to the maximum activity of 8000 TU detected at Belukha glacier, 350 km to the northwest [*Olivier et al.*, 2004], for location see Figure 1. Similar high values at both sites are due to enhanced stratosphere-troposphere transport of ^{3}H in spring/summer, the seasons when precipitation is occurring.

Major volcanic eruptions have large climatic impacts through the emission of sulfur dioxide into the stratosphere, where it is oxidized to sulfate aerosols which influence the earth radiative balance [*Robock and Jianping*, 1995]. These eruptions are often used as time markers in ice cores [e.g. *Robock and Jianping*, 1995; *Zielinski*, 1995]. However, sulfate has various sources, the major ones being anthropogenic sulfur dioxide emissions from fossil fuel combustion and natural emissions of mineral dust containing gypsum. In order to correct for the mineral sulfate input an alternative non-dust sulfate record is required. Calcium was used as tracer for mineral dust and by regression analysis of sulfate and calcium concentrations prior to significant fossil fuel emissions (1945 AD), a ratio of 0.22 was obtained (concentration in $\mu eq\ l^{-1}$). This value is very similar to the value 0.21 deduced at Belukha [*Olivier et al.*, 2006]. As long as other sources are negligible, maxima in the non-dust sulfate ([non-dust sulfate] = [sulfate] - 0.22[calcium]) can be related to volcanic eruptions [*Zielinski*, 1995] as shown in Figure 4. Strong anthropogenic sulfate concentrations prevent an unambiguous identification of volcanic eruptions in the upper 20 m weq, corresponding to the period 2009 to 1941. Hence, potential signals of the Pinatubo (1991), El Chichon (1982), and Agung (1963) eruptions could not be attributed. Four eruptions were identified in the non-dust sulfate record: Cerro Azul (1933), Katmai (1912), Shiveluch (1854), and Tambora (1815). Remarkable is the strength of the 1815 Tambora eruption with its signal even exceeding the anthropogenic emissions. A similarly pronounced 1815 Tambora signal was observed at the Belukha glacier in the Siberian Altai [*Olivier et al.,* 2006], reinforcing the dating for both ice cores. Older eruptions could not be clearly identified, which requires more than one sample with elevated sulfate concentration, due to an attenuation of the signal by

295 annual layer thinning. Elevated concentrations of the non-dust record for the
296 lowest cm are not attributed to a volcanic eruption but are rather an artifact of
297 the nearby bedrock.
298
299 *4.2 Annual layer counting*
300 To obtain a continuous age-depth relation and to account for interannual
301 accumulation variations, annual layer counting (ALC) was performed using the
302 record of seasonally varying parameters ($\delta^{18}O$, concentration of formate and
303 ammonium). This method has been successfully applied before in ice core
304 science [e.g. *Cole-Dai et al.*, 1997; *Olivier et al.*, 2006]. On average one year
305 contains 9 to 10 samples, ranging from 30 at the top to 2 samples at 36 m weq,
306 the year 1815. Below this depth recognition of annual cycles and allocation of
307 volcanic eruptions was not possible since the sampling resolution could not be
308 increased further for adjusting to the strong annual-layer thinning. The
309 uncertainty of ALC was established through repeated counting. Within one
310 decade of an identified horizon an error of ±1 year was estimated increasing to
311 ±2-3 years outside of these ranges (1998-1974, 1952-1944, 1902-1865, 1843-
312 1826). Chemical tracers are independent of the $\delta^{18}O$ record, which further
313 increases the robustness of the ALC.
314
315 *4.3 Radioactive dating with ^{210}Pb*
316 To obtain an additional and independent timescale, ^{210}Pb activity was analyzed
317 in the ice. This technique allows dating on a centennial timescale determined by
318 the half-life of ^{210}Pb ($t_{1/2}$ = 22.3 years) and has been applied before for ice cores
319 [e.g. *Gäggeler et al.*, 1983; *Eichler et al.*, 2000]. The decreasing activity with depth

was used to establish an age-depth relation, assuming constant input of ^{210}Pb and no post-depositional alteration. Figure 5 shows the decrease of ^{210}Pb activity concentration and the corresponding age increase with depth. The values range from 1.7 to 387 mBq l^{-1} with an error of 1.7 to 14.6% depending on the counting statistics. The scatter of the data in the uppermost 15 m weq can partly be explained by deviation of the assumed constant input. With increasing depth the nonlinear activity-depth relation confirms the annual-layer thinning for the lower part of the glacier. The ^{210}Pb surface activity in the Tsambagarav mountain range is 272 mBq l^{-1}, obtained by applying a linear regression to the upper 20 m weq and defining the y intercept as surface activity. This approach neglects compaction of the annual layers for this section. The value is identical with the surface activity at the Belukha glacier (280 mBq l^{-1}) [*Olivier et al.*, 2006], but much higher than in less continental areas such as the Alps (85 mBq l^{-1}, [*Eichler et al.,* 2000]). High surface activity allowed dating back to 1853 ± 5 AD. The period 1815-2009 AD was thus dated by four independent techniques, which agree well. The ^{3}H fallout in 1963, major volcanic eruptions and ALC dates are all located within the uncertainty of the ^{210}Pb values (see Figure 5).

4.4 Glacier flow model

A further method to establish an age-depth scale is the application of a simple glacier flow model given by

$$z(t) = H\left[1 - \left(\frac{t \cdot b \cdot p}{H} - 1\right)^{-1/p}\right] \qquad (1)$$

where H is the glacier thickness (58 m weq), z the depth in water equivalent, t the time, b the modeled averaged accumulation rate, and p a constant [*Thompson*

344 *et al.*, 1990]. Dated horizons and ALC were used to fit *b* and *p* in Equation 1
345 (R^2=0.998). The flow model reproduces well the timescale derived by the
346 combination of the different dating methods (Figure 5). Thus, the upper 36 m
347 weq of the Tsambagarav ice core give a consistent age-depth relation with
348 annual resolution.
349
350 **5 *Millennial ice from the Mongolian Altai***
351 *5.1 Complex age-depth relation derived from ^{14}C data*
352 To establish a timescale for the lower part of the ice core, a radiocarbon method
353 for dating ice developed by our group was applied [*Jenk et al.*, 2009; *Kellerhals et*
354 *al.*, 2010]. From a total of ten radiocarbon samples, the uppermost two were
355 analyzed to investigate a possible offset in the transition from the upper to the
356 lower part of the ice core caused by an initial age of the carbonaceous particles
357 (inbuilt ^{14}C). The eight remaining samples were used to date the ten meters weq
358 above bedrock. The age ranges of the top two samples (ETH43436.1.1,
359 ETH43438.1.1) at 38.19 and 41.64 m weq are 280 to 10 and 270 to 10 cal years
360 BP, respectively. This large relative uncertainty has two reasons: First, the ages
361 are at the upper boundary of the radiocarbon method (<500 cal years BP, [*Jenk et*
362 *al.*, 2009]), which is determined by the potential influence from fossil fuel
363 emissions, and second the scattering of the radiocarbon calibration curve in this
364 period. Because of this large uncertainty the two ages cannot be distinguished.
365 Nevertheless, the horizon of the 1815 Tambora eruption lies within the 1σ-range
366 of the ^{14}C ages making a dating offset between the methods used in the upper
367 and lower part of the ice core unlikely. Therefore the ^{14}C values seem to be
368 suitable to establish an age-depth relation for the lower part of the ice core.

Given that, the ^{14}C ages show a steady increase for the section 36 m weq down to bedrock (Table I), reinforcing the suitability of the method. The 68% range is relatively small, due to good AMS measurement performance, little scatter in the calibration curve, and large sample sizes. The concentrations of particulate organic carbon varied from 116 to 340 μg l^{-1}, resulting in absolute carbon amounts well above the limit of the method (3 μg, [*Sigl et al.,* 2009]). For the sections 36 to 52 m weq the values indicate faster layer thinning than predicted by commonly used age-depth models ([*Nye*, 1963; *Thompson et al.*, 1990]; see 4.4, Figure 5). This characteristic has been noticed before for other midlatitude glaciers frozen to bedrock [*Thompson et al.*, 1998; *Knüsel et al.*, 2003]. An alternative age-depth model is thus required to fit the discrete ^{14}C ages and obtain a continuous timescale. Analogous to the approach used in *Thompson et al.*, [1998] an empirical exponential equation given by

$$z(t) = a \cdot e^{b \cdot t} + c \cdot e^{d \cdot t} \qquad (2)$$

was derived, where z is the depth in m weq, t the time in years BP, and a-d are constants. The equation has been applied for the lower part of the ice core and therefore only valid for z > 36 m weq. Nine horizons were used to fit the equation, including the 1815 Tambora eruption and the eight lower ^{14}C ages. The considered horizons are well reproduced by the equation (R^2=0.997) with an almost perfect match of the 1815 Tambora eruption leading to a smooth transition from the upper to the lower part of the ice core (Figure 5). The model uncertainty was determined by two alternative datasets. The lower (upper) limit of the model was calculated by fitting Equation 2 with the 1815 Tambora eruption and the ^{14}C ages minus (plus) one standard deviation. The empirical exponential equation provides a monotonic age-depth model and avoids

394 constant layer thickness between two time horizons, which would lead to a
395 stepwise function implying abrupt changes in layer thickness. Since the glacier
396 flow model (Equation 1) approaches asymptotically the depth of 58 m weq, the
397 intersection with the empirically derived timescale (Equation 2) is located at
398 57.6 m weq predicting identical age at bedrock.
399
400 *5.2 Neoglacial ice at bedrock*
401 The ^{14}C dates revealed a basal age of 5920 to 5660 cal years BP. Sufficient carbon
402 content gives a confident value with a small relative uncertainty. This age of the
403 deepest ice close to bedrock suggests ice-free conditions prior to approximately
404 6000 years BP at 4100 m asl on the summit of Khukh Nuru Uul. Complete
405 disappearance of glaciers during the HCO has been identified in various glaciated
406 areas of the globe [*Solomina et al.*, 2008; *Davis et al.*, 2009]. The disappearance of
407 the tropical glaciers in the Andes has been explained through a combination of
408 increasing temperatures and most notably a decrease in precipitation [*Abbott et*
409 *al.*, 2003]. Also in Scandinavia most of the glaciers melted away during the mid
410 Holocene mainly because of increased temperatures [*Nesje*, 2009] and there is
411 evidence that also in the High Arctic ice caps had disappeared [*Madsen and*
412 *Thorsteinsson*, 2001].
413 The maximal ice age of 6000 years BP can be interpreted as glacier advance
414 following the HCO and provides indication for the onset of the Neoglaciation. The
415 timing is consistent with glacier waxing in northwestern China (5680 years BP,
416 [*Zhou et al.*, 1991]), implying that this feature of Neoglaciation is more than only
417 a local phenomenon of the Mongolian Altai, and corroborating the findings of this
418 study. Complete glacier vanishing was also suggested for the Russian Altai by

7000 years BP, however the advance occurred later, around 5000 years BP [*Agatova et al.*, 2012].

This is the first study documenting the end of the HCO and the onset of Neoglaciation in the Mongolian Altai. There is strong evidence that the top of Khukh Nuru Uul was ice free until roughly 6000 years BP, pointing towards glacier-hostile climatic conditions during the HCO, inducing a minimum ELA-shift of 430 m from 3700 to 4130 m. Extrapolating this increase in ELA to the surrounding glaciated areas results in a complete degradation of the Mongolian glaciers south of the Tsambagarav mountain range where the altitude difference between ELA and summit is today smaller than 430 m. To the north glaciers must at least have declined severely, as an ELA increase of 430 m would in the present conditions not be sufficient for complete degradation. This approach is conservative since the upper limit of the ELA-shift is defined by the elevation of Khukh Nuru Uul and might have been larger. Nevertheless the possibility remains that glaciers located on north facing slopes survived the ELA increase. This study therefore suggests, that most of the current glaciers in the Mongolian Altai are not remnants of the Last Glacial Maximum but have been formed during the second part of the Holocene.

6 *Accumulation reconstruction*

6.1 Accumulation rates for the period 1815 to 2009 AD

Annual accumulation rates can be reconstructed based on ALC combined with flow models to correct for the nonlinear thinning. The flow model used to date the upper part of the ice core (Equation 1, [*Thompson et al.*, 1990]) provides an adequate thinning rate. The accumulation was calculated from the ratio of the

measured annual layer thickness obtained by ALC to the modeled thickness multiplied by the surface accumulation rate. Neglecting lateral flow within the upper 3.35 m weq (covering a period of 10 years) yields a surface accumulation rate of 335 mm. For the period 1815 to 2009 AD the reconstructed mean annual accumulation rate is 329 mm weq with a standard deviation of 91 mm. The profile shows no trend although drier decades are identifiable around 1950 and 1910 AD (Figure 6). The mean value is in good agreement with the surface accumulation of 335 mm and appears plausible in comparison with precipitation in the lowlands of less than 200 mm. This is the first study providing glacier accumulation estimations for the last 200 years in the Mongolian Altai.

6.2 Accumulation trends for the past 6 kyr

For the lower 20 m weq another approach was required to reconstruct the accumulation since the derived age-depth relation (Equation 1) deviates from the age-depth model (Equation 2; Figure 5). Within the section 45 to 52 m weq the age-depth function suggests a more rapid thinning of the annual layers relative to the lowest six m weq. Changes in the accumulation rate are one possible explanation for this characteristic. To account for these fluctuations another approach was applied by a stepwise calculation of the accumulation rate accumulation (b_{ij}) between two dated horizons *i* and *j* resulting in a function given by

$$b_{ij} = \frac{1}{\Delta t_{ij}} \int_{z_i}^{z_j} \left(1 - \frac{z}{H}\right)^{-p} dz \quad (3)$$

where Δt_{ij} is the number of years between z_i and z_j analogous to [*Thompson et al.*, 1998]. In order to better describe the observed fluctuation in layer thinning,

468 different parameters *p* (0.7, 1.1 and 1.3) were used representing weak, medium,
469 and strong thinning resulting in three time series of accumulation according to
470 *Thompson et al.* [1998]. The reconstructed accumulation rates differ largely with
471 varying *p* yet following a similar trend. Figure 6 shows three distinct phases of
472 high, low, and again high accumulation rates. The last 250 years indicate wetter
473 conditions than the preceding 4500 years. During the period 800 to 4700 years
474 BP accumulation rates were considerably lower than in the preceding and
475 following period. Data close to bedrock suggest an increase in humidity from
476 4800 to 6000 years BP. A precipitation reconstruction from the Karakorum
477 claims the period 1850 AD to present to be the wettest within the past millennia
478 [*Treydte et al.*, 2006], a conclusion supporting the elevated accumulation rates
479 from 1800 to 2009 AD in Mongolia. Lake sediment records [*Rudaya et al.*, 2009]
480 show analogous to the ice core data, that present conditions in the Mongolian
481 Altai are wetter than during the past millennia. In accordance with our
482 accumulation reconstruction *Wanner et al.* [2011] proposed a shift of the
483 Intertropical Convergence Zone (ITCZ) between the HCO and the Neoglaciation
484 to explain drastic changes in the precipitation pattern north of the Himalaya. Dry
485 conditions for the same period have also been suggested for the Russian and
486 Mongolian Altai [*Rudaya et al.*, 2009; *Agatova et al.*, 2012]. Noticeable is the
487 persistence of dry conditions, lasting until the beginning of the Medieval Climate
488 Anomaly (AD 950 to 1250).
489
490 ***7 Conclusions***
491 The Tsambagarav ice core was dated with a variety of methods, including
492 identification of reference horizons, annual layer counting, nuclear dating with

493 ^{210}Pb, and a novel ^{14}C technique. This gives confidence in the obtained
494 chronology. The upper 36 m weq embody 200 years of climate information,
495 suitable for climate reconstruction with annual resolution. Strong annual layer
496 thinning characterizes the lower 20 m weq. To obtain a continuous age-depth
497 profile an empirical equation was implemented, linking the upper and lower part
498 of the ice core.
499 The accumulation reconstruction indicates changes in the precipitation pattern
500 over the last 6000 years. The most recent 200 years are influenced by relative
501 wet conditions, preceded by a dry period beginning around 5000 years BP.
502 During the build-up of the glacier 6000 years BP the derived accumulation
503 suggests an increase in precipitation. This is in agreement with other
504 reconstructions, pointing to a consistent precipitation evolution for the Altai
505 region.
506 Dating of the basal ice revealed a build-up of the glacier at roughly 6000 years
507 BP. This result suggests complete glacier disappearance during the HCO as
508 observed in various other places of the globe. The waxing of the glacier provides
509 benchmarks for the end of the HCO and the onset of the Neoglaciation at around
510 6000 years BP. The total glacier disappearance indicates higher temperatures at
511 that time compared to nowadays, especially since the period preceding the
512 Neoglaciation experienced wet climatic conditions. High accumulation during the
513 build-up of the glacier combined with decreasing temperatures is a plausible
514 hypothesis for the onset of the glaciers in the Tsambagarav mountain range. A
515 minimal ELA-shift of 430 m on Khukh Nuru Uul is seen as a strong indication that
516 most glaciers in the Mongolian Altai had also disappeared. Accordingly, most
517 glaciers in the Mongolian Altai are not remnants of the Last Glacial Maximum, but

instead they were formed during the second part of the Holocene. This provides new insight into the glaciation/deglaciation process of the Mongolian Altai.

Acknowledgements

This project was supported by the Swiss National Science Foundation (200021_119743) and the Russian Academy of Sciences (Integration project No. 92 of SB RAS and project 16.12 of Presidium RAS). We are much indebted to Sergey Mironov, Chairman of the Council of the Federal Assembly of the Russian Federation for assistance in organizing our expedition and to the Federal Security Service of the Russian Federation for flying us safely to the glacier. The support of Dr Beket from the Social Economy Research Center in Bayan-Ulgii, Mongolia, and Veronica Morozova from IWEP is highly acknowledged. We thank Beat Rufibach, Michael Sigl, Manuel Schläppi, and Heinz Gäggeler for their help in drilling the ice core. Jost Eikenberg (Paul Scherrer Institut) for ^{3}H analysis, Edith Vogel (University of Bern) for ^{210}Pb sample preparation, Sönke Szidat (University of Bern) for access to the Theodore system, and Lukas Wacker (ETH Zürich) for help with the AMS analysis are highly acknowledged.

References:

Abbott, M. B., B. B. Wolfe, A. P. Wolfe, G. O. Seltzer, R. Aravena, B. G. Mark, P. J. Polissar, D. T. Rodbell, H. D. Rowe, and M. Vuille (2003), Holocene paleohydrology and glacial history of the central Andes using multiproxy lake sediment studies, *Palaeogeography, Palaeoclimatology, Palaeoecology*, *194*(1-3), 123–138, doi:10.1016/S0031-0182(03)00274-8.

Agatova, A., A. Nazarov, and R. Nepop (2012), Holocene glacier fluctuations and climate changes in the southeastern part of the Russian Altai (South Siberia) based on a radiocarbon chronology, *Quaternary Science Reviews*, *43*(0), 74–93, doi: 10.1016/j.quascirev.2012.04.012.

Arendt, A. et al. (2012), Randolph Glacier Inventory [v2.0]: A Dataset of Global Glacier Outlines. Global Land Ice Measurements from Space, Boulder Colorado, USA. Digital Media.

Bond, G., W. Showers, M. Cheseby, R. Lotti, P. Almasi, P. de Menocal, P. Priore, H.

548 Cullen, I. Hajdas, and G. Bonani (1997), A Pervasive Millennial-Scale Cycle in
549 North Atlantic Holocene and Glacial Climates, *Science*, *278*(5341), 1257–
550 1266, doi:10.1126/science.278.5341.1257.

551 Cole-Dai, J., E. Mosley-Thompson, and L. Thompson (1997), Annually resolved
552 southern hemisphere volcanic history from two Antarctic ice cores, *J.*
553 *Geophys. Res.*, *102*(D14), 16761–16771, doi: 10.1029/97JD01394

554 D'Arrigo, R., G. Jacoby, D. Frank, N. Pederson, E. Cook, B. Buckley, B. Nachin, R.
555 Mijiddorj, and C. Dugarjav (2001), 1738 years of Mongolian temperature
556 variability inferred from a tree-ring width chronology of Siberian pine,
557 *Geophys. Res. Lett.*, *28*(3), 543–546, doi:10.1029/2000GL011845.

558 Davis, P. T., B. Menounos, and G. Osborn (2009), Holocene and latest Pleistocene
559 alpine glacier fluctuations: a global perspective, *Quaternary Science Reviews*,
560 *28*(21-22), 2021–2033, doi:10.1016/j.quascirev.2009.05.020.

561 Demberel, O. (2011), Sovremennoe Oledenje Gornogo Uzla Tsambagarav Ul
562 (Mongolskiy Altay) (Present day glaciation of the Tsambagarav mountain
563 massive, Mongolian Altai), Vestnik Tomskogo Gosudarstvenogo Universiteta,
564 vol. 348, http://sun.tsu.ru/mminfo/000063105/348/348.html

565 Eichler, A., M. Schwikowski, and H. W. Gäggeler (2000), Glaciochemical dating of
566 an ice core from upper Grenzgletscher (4200 m asl), *Journal of Glaciology*,
567 *46*(154), 507–515, doi: 10.3189/172756500781833098.

568 Eichler, A., S. Brütsch, S. Olivier, T. Papina, and M. Schwikowski (2009a), A 750
569 year ice core record of past biogenic emissions from Siberian boreal forests,
570 *Geophys. Res. Lett.*, *36*(18), L18813, doi:10.1029/2009GL038807.

571 Eichler, A., S. Olivier, K. Henderson, A. Laube, J. Beer, T. Papina, H. W. Gäggeler,
572 and M. Schwikowski (2009b), Temperature response in the Altai region lags
573 solar forcing, *Geophys. Res. Lett.*, *36*(1), L01808, doi:10.1029/2008GL035930.

574 Eichler, A., W. Tinner, S. Brütsch, S. Olivier, T. Papina, and M. Schwikowski
575 (2011), An ice-core based history of Siberian forest fires since AD 1250,
576 *Quaternary Science Reviews*, *30*(9–10), 1027–1034,
577 doi:10.1016/j.quascirev.2011.02.007.

578 Gäggeler, H., H. R. von Gunten, E. Rössler, and H. Oeschger (1983), ^{210}Pb-Dating of
579 cold Alpine firn/ice cores from Colle Gnifetti , Switzerland, *Journal of*
580 *Glaciology*, *29*(101), 165–177.

581 Ginot, P., F. Stampfli, D. Stampfli, M. Schwikowski, and H. Gaggeler (2002),
582 FELICS, a new ice core drilling system for high-altitude glaciers, *Proceedings*
583 *of the workshop "Ice Drilling Technology 2000," Memoirs of National Institute*
584 *of Polar Research, Special Issue*, *56*, 38–48.

585 Grosjean, M., P. J. Suter, M. Trachsel, and H. Wanner (2007), Ice-borne prehistoric
586 finds in the Swiss Alps reflect Holocene glacier fluctuations, *J. Quaternary Sci.*,
587 *22*(3), 203–207, doi:10.1002/jqs.1111.

588 Henderson, K., A. Laube, H. Gäggeler, and S. Olivier (2006), Temporal variations
589 of accumulation and temperature during the past two centuries from
590 Belukha ice core, Siberian Altai, *J. Geophys. Res.*, *111*(D3), D03104,
591 doi:1029/2005JD005819

592 Ivy-Ochs, S., H. Kerschner, M. Maisch, M. Christl, P. W. Kubik, and C. Schlüchter
593 (2009), Latest Pleistocene and Holocene glacier variations in the European
594 Alps, *Quaternary Science Reviews*, *28*(21–22), 2137–2149,
595 doi:10.1016/j.quascirev.2009.03.009.

596 Jenk, T. M., S. Szidat, D. Bolius, M. Sigl, H. W. Gäggeler, L. Wacker, M. Ruff, C.
597 Barbante, C. F. Boutron, and M. Schwikowski (2009), A novel radiocarbon
598 dating technique applied to an ice core from the Alps indicating late
599 Pleistocene ages, *J. Geophys. Res.*, *114*(D14), D14305,
600 doi:10.1029/2009JD011860.

601 Johnsen, S. J. et al. (1997), The $\delta^{18}O$ record along the Greenland Ice Core Project
602 deep ice core and the problem of possible Eemian climatic instability, *J.*
603 *Geophys. Res.*, *102*(C12), 26397–26410, doi:10.1029/97JC00167.

604 Kellerhals, T., S. Brütsch, M. Sigl, S. Knüsel, H. W. Gäggeler, and M. Schwikowski
605 (2010), Ammonium concentration in ice cores: A new proxy for regional
606 temperature reconstruction? *J. Geophys. Res.*, *115*(D16), D16123,
607 doi:10.1029/2009JD012603.

608 Klinge, M., J. Böhner, and F. Lehmkuhl (2003), Climate pattern, snow- and
609 timberlines in the Altai Mountains, Central Asia, *Erdkunde*, *57*(4), 296–308.

610 Knüsel, S., P. Ginot, U. Schotterer, M. Schwikowski, H. W. Gäggeler, B. Francou, J.
611 R. Petit, J. C. Simoes, and J. D. Taupin (2003), Dating of two nearby ice cores
612 from the Illimani, Bolivia, *J. Geophys. Res.*, *108*(D6), 4181,
613 doi:10.1029/2001JD002028.

614 Lehmkuhl, F. (1998), Quaternary glaciations in central and western Mongolia, *J.*
615 *Quaternary Sci.*, *13*(6), 153–167.

616 Lehmkuhl, F., and L. Owen (2005), Late Quaternary glaciation of Tibet and the
617 bordering mountains: a review, *Boreas*, *34*(2), 87–100,
618 doi:10.1080/03009480510012908.

619 Lehmkuhl, F., M. Klinge, and G. Stauch (2011), The Extent and Timing of Late
620 Pleistocene Glaciations in the Altai and Neighbouring Mountain Systems, in
621 Ehlers, H. J., Gibbard P. L., Hughes, P. D. (Eds), *Developments in Quaternary*
622 *Sciences*, Volume 15, Elsevier, pp. 967–979, doi: 10.1016/B978-0-444-
623 53447-7.00069-6.

624 Loader, N., G. Helle, S. Los, and F. Lehmkuhl (2010), Twentieth-century summer
625 temperature variability in the southern Altai Mountains: A carbon and
626 oxygen isotope study of tree-rings, *The Holocene*, *20*(7), 1149–1156,
627 doi:10.1177/0959683610369507.

628 Mackay, A. W. et al. (2012), Aquatic ecosystem responses to Holocene climate
629 change and biome development in boreal, central Asia, *Quaternary Science*
630 *Reviews*, *41*(0), 119–131, doi: 10.1016/j.quascirev.2012.03.004.

631 Madsen, K., and T. Thorsteinsson (2001), Textures, fabrics and meltlayer
632 stratigraphy in the Hans Tausen ice core, North Greenland - indications of
633 late Holocene ice cap genration?, in *(U.C. Hammer, ed.) The Hans Tausen Ice*
634 *Cap Glaciology and Glacial Geology*, vol. 39, pp. 97–114, Meddelelser om
635 Grønland, Geoscience.

636 Mayewski, P. A. et al. (2004), Holocene climate variability, *Quaternary Research*,
637 *62*(3), 243–255, doi:10.1016/j.yqres.2004.07.001.

638 Miller, G. H. et al. (2012), Abrupt onset of the Little Ice Age triggered by
639 volcanism and sustained by sea-ice/ocean feedbacks, *Geophys. Res. Lett.*,
640 *39*(2), L02708, doi:10.1029/2011GL050168.

641 Nesje, A. (2009), Latest Pleistocene and Holocene alpine glacier fluctuations in
642 Scandinavia, *Quaternary Science Reviews*, *28*(21–22), 2119–2136,
643 doi:10.1016/j.quascirev.2008.12.016.

644 Nesje, A., L. H. Pilo, E. Finstad, B. Solli, V. Wangen, R. S. Odegard, K. Isaksen, E. N.
645 Storen, D. I. Bakke, and L. M. Andreassen (2012), The climatic significance of
646 artefacts related to prehistoric reindeer hunting exposed at melting ice
647 patches in southern Norway, *The Holocene*, *22*(4), 485–496,
648 doi:10.1177/0959683611425552.

649 Nye, J. (1963), Correction factor for accumulation measured by the thickness of
650 the annual layers in an ice sheet, *Journal of Glaciology*, *4*(36), 785–788.

651 Oerlemans, J. (2005), Extracting a climate signal from 169 glacier records,
652 *Science*, *308*(5722), 675–677, doi:10.1126/science.1107046.

653 Olivier, S., C. Blaser, S. Brütsch, N. Frolova, H. W. Gäggeler, K. A. Henderson, A. S.
654 Palmer, T. Papina, and M. Schwikowski (2006), Temporal variations of
655 mineral dust, biogenic tracers, and anthropogenic species during the past
656 two centuries from Belukha ice core, Siberian Altai, *J. Geophys. Res.*, *111*(D5),
657 D05309, doi:10.1029/2005JD005830.

658 Olivier, S., S. Bajo, L. K. Fifield, H. W. Gäggeler, T. Papina, P. H. Santschi, U.
659 Schotterer, M. Schwikowski, and L. Wacker (2004), Plutonium from global
660 fallout recorded in an ice core from the Belukha glacier, Siberian Altai,
661 *Environmental Science & Technology*, *38*(24), 6507–6512,
662 doi:10.1021/es0492900.

663 Owen, L. A. (2009), Latest Pleistocene and Holocene glacier fluctuations in the
664 Himalaya and Tibet, *Quaternary Science Reviews*, *28*(21–22), 2150–2164,
665 doi:10.1016/j.quascirev.2008.10.020.

666 Ramsey, C. (2001), Development of the radiocarbon calibration program,
667 *Radiocarbon*, *43*(2A, Part 1), 355–363.

668 Reimer, P. J. et al. (2009), Intcal09 and marine09 radiocarbon age calibration
669 curves, 0-50,000 years cal bp, *Radiocarbon*, *51*(4), 1111–1150.

670 Robock, A., and M. Jianping (1995), The volcanic signal in surface temperature
671 observations, *Journal of Climate*, *8*, 1086–1103, doi:10.1175/1520-
672 0442(1995)008<1086:TVSIST>2.0.CO;2

673 Rudaya, N. et al. (2009), Holocene environments and climate in the Mongolian
674 Altai reconstructed from the Hoton-Nur pollen and diatom records: a step
675 towards better understanding climate dynamics in Central Asia, *Quaternary*
676 *Science Reviews*, *28*(5–6), 540–554, doi: 10.1016/j.quascirev.2008.10.013.

677 Ruff, M., L. Wacker, H. W. Gäggeler, M. Suter, H.-A. Synal, and S. Szidat (2007), A
678 gas ion source for radiocarbon measurements at 200 kV, *Radiocarbon*, *49*(2),
679 307–314, doi:10.2458/rc.v49i2.2930.

680 Schotterer, U., K. Fröhlich, H. W. Gäggeler, S. Sandjordj, and W. Stichler (1997),
681 Isotope records from Mongolian and Alpine ice cores as climate indicators,
682 *Climatic Change*, *36*(3), 519–530, doi:10.1023/A:1005338427567.

683 Sigl, M., et al. (2009), Towards radiocarbon dating of ice cores, *Journal of*
684 *Glaciology*, *55*(194), 985–996.

685 Solomina, O., W. Haeberli, C. Kull, and G. Wiles (2008), Historical and Holocene
686 glacier–climate variations: General concepts and overview, *Global and*
687 *Planetary Change*, *60*(1-2), 1–9, doi:10.1016/j.gloplacha.2007.02.001.

688 Synal, H.-A., M. Stocker, and M. Suter (2007), MICADAS: A new compact
689 radiocarbon AMS system, *Nuclear Instruments and Methods in Physics*
690 *Research Section B: Beam Interactions with Materials and Atoms*, *259*(1), 7–
691 13, doi:10.1016/j.nimb.2007.01.138.

692 Szidat, S., T. M. Jenk, H. W. Gäggeler, H.-A. Synal, I. Hajdas, G. Bonani, and M.
693 Saurer (2004), THEODORE, a two-step heating system for the EC/OC
694 determination of radiocarbon (^{14}C) in the environment, *Nuclear Instruments*
695 *and Methods in Physics Research Section B: Beam Interactions with Materials*
696 *and Atoms*, *223–224*(0), 829–836, doi: 10.1016/j.nimb.2004.04.153.

697 Thompson, L. G. et al. (1998), A 25,000-year tropical climate history from
698 Bolivian ice cores, *Science*, *282*(5395), 1858–1864,
699 doi:10.1126/science.282.5395.1858.

700 Thompson, L. G., E. Mosley-Thompson, M. Davis, J. F. Bolzan, J. Dai, L. Klein, N.
701 Gundestrup, T. Yao, X. Wu, and Z. Xie (1990), Glacial stage ice core records
702 from the subtropical Dunde ice cap, China, *Annals of Glaciology*, *14*, 288–297.

703 Treydte, K. S., G. H. Schleser, G. Helle, D. C. Frank, M. Winiger, G. H. Haug, and J.
704 Esper (2006), The twentieth century was the wettest period in northern
705 Pakistan over the past millennium, *Nature*, *440*(7088), 1179–1182,
706 doi:10.1038/nature04743.

Wanner, H., O. Solomina, M. Grosjean, and S. Ritz (2011), Structure and origin of Holocene cold events, *Quaternary Science Reviews*, *30*(21-22), 3109–3123, doi:10.1016/j.quascirev.2011.07.010.

Zhou, S., F. Chen, B. Pan, J. Cao, J. Li, and E. Derbyshire (1991), Environmental change during the Holocene in western China on a millennial timescale, *The Holocene*, *1*(2), 151–156, doi: 10.1177/095968369100100207.

Zielinski, G. A. (1995), Stratospheric loading and optical depth estimates of explosive volcanism over the last 2100 years derived from the Greenland Ice Sheet Project 2 ice core, *J. Geophys. Res.*, *100*(D10), 20937–20955, doi:10.1029/95JD01751.

Table I: Summary of the ^{14}C results for the Tsambagarav 2009 ice core samples, analyzed at ETH Zürich. The fraction of modern (f_M) is given with the corresponding 1σ-range. For the calibrated age, ranges are given with 68% probability. All the values correspond to the particulate organic carbon (POC) fraction of the sample.

Figure 1: (a) Location of the Tsambagarav mountain range (red star), lake sediment Hoton-Nur (black star) in Mongolia, and Belukha glacier in the Siberian Altai (blue star; http://www.geomapapp.org). (b) Landsat images with SRTM DHM elevations (solid lines 100 m intervals), the red rectangle corresponds to the area of detailed glaciological survey. (c) Landscape of the Tsambagarav mountain range in the southern Mongolian Altai with typical small ice caps. View to the southeast from close to the drill site towards the campsite. Photo: H. Machguth.

Figure 2: (a) Radar profie recorded at Khukh Nuru Uul with clearly identifiable bedrock at 70 m depth (yellow arrow symbolize drilling location). (b) Surface and bed topography at the drill site; the core is indicated by the dashed red line.

Figure 3: Density (blue) and temperature (red) profile of Khukh Nuru Uul glacier.

Figure 4: Evolution of the ^{3}H activity in Tritium Units (TU) with depth in the Tsambagarav ice core for coarse (red) and fine (green) resolution decay corrected for the year 1963. Non-dust sulfate record in $\mu eq\ l^{-1}$ (blue) with the corresponding volcanic eruptions, 1933 Cerro Azul (1), 1912 Katmai (2), 1854 Shiveluch (3), and 1815 Tambora (4). The elevated concentrations in the upper 19 m weq are due to anthropogenic fossil fuel combustion (grey curve).

Figure 5: Age-depth relation for the Tsambagarav ice core. Annual layer counting (green crosses), tritium peak (yellow diamond), volcanic eruptions (blue triangle), ^{210}Pb activity with analytical uncertainties (red circles), glacier flow model (blue dashed line), exponential equation (black dashed line) with upper and lower limit of the equation (grey shaded area) and ^{14}C values with the 1σ-range (black squares). Insert: magnification of the lower 36 m weq with identical symbols.

Figure 6: (a) Accumulation profile for the period 1825 to 2009 AD in m weq with 1σ uncertainties. (b) Accumulation reconstruction presented as anomaly from the mean for the past 6 kyr. The three age-depth models representing weak, medium, and strong thinning were combined and presented as deviation from the mean.

Table

Core segment #	Depth	Ice	Absolute carbon amount	AMS Lab Nr.	Radiocarbon	Calibrated age
	m weq	**kg**	**µg**		f_M	**years BP = 1950**
75	38.19	0.166	33	ETH43436.1.1	0.983±0.012	280-10
81	41.64	0.181	19	ETH43438.1.1	0.996±0.017	270-10
92	47.55	0.219	33	ETH42822.1.1	0.891±0.010	930-770
97	49.65	0.183	32	ETH42824.1.1	0.800±0.010	1860-1570
102	52.21	0.186	22	ETH42826.1.1	0.666±0.014	3720-3270
105-1	53.59	0.278	58	ETH42156	0.605±0.007	4800-4420
105-2	53.73	0.229	29	ETH42166	0.597±0.010	4850-4240
107	55.05	0.143	23	ETH42828.1.1	0.578±0.015	5440-4710
109	55.80	0.194	32	ETH42157	0.548±0.009	5710-5330
111	57.45	0.161	55	ETH42836.1.1	0.532±0.008	5920-5660

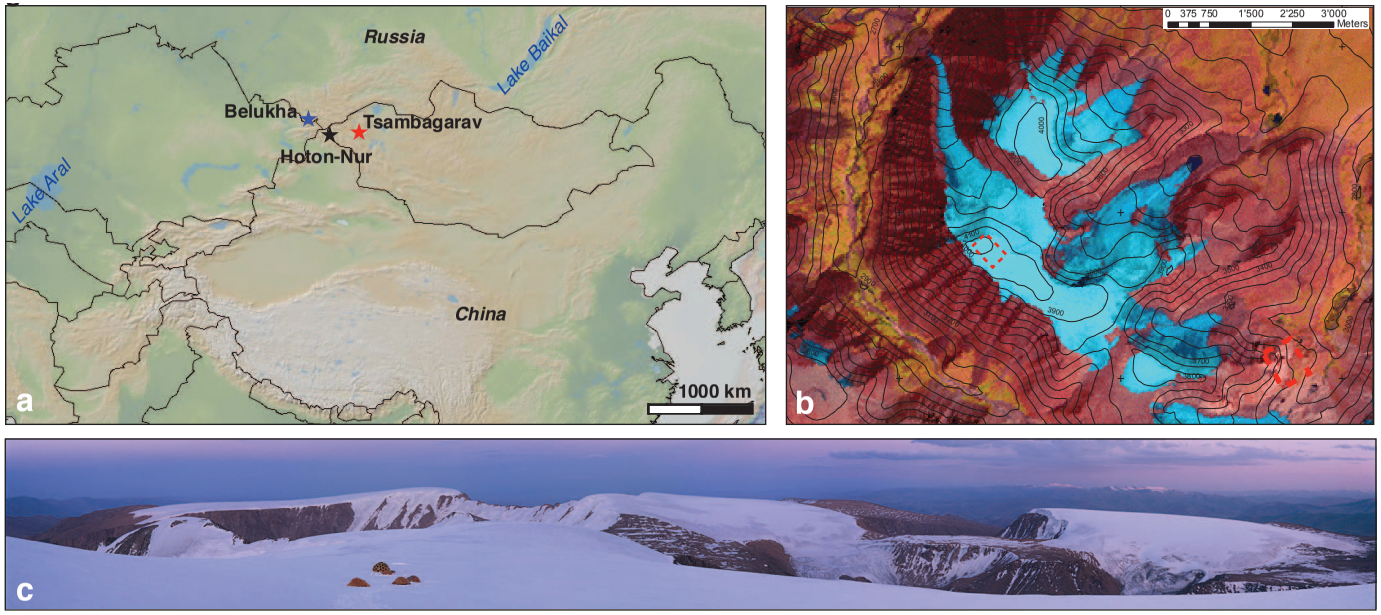
Russia
Lake Baikal
Belukha
Tsambagarav
Hoton-Nur
Lake Aral
China
1000 km
a
0 375 750 1'500 2'250 3'000
Meters
b
c

Figure

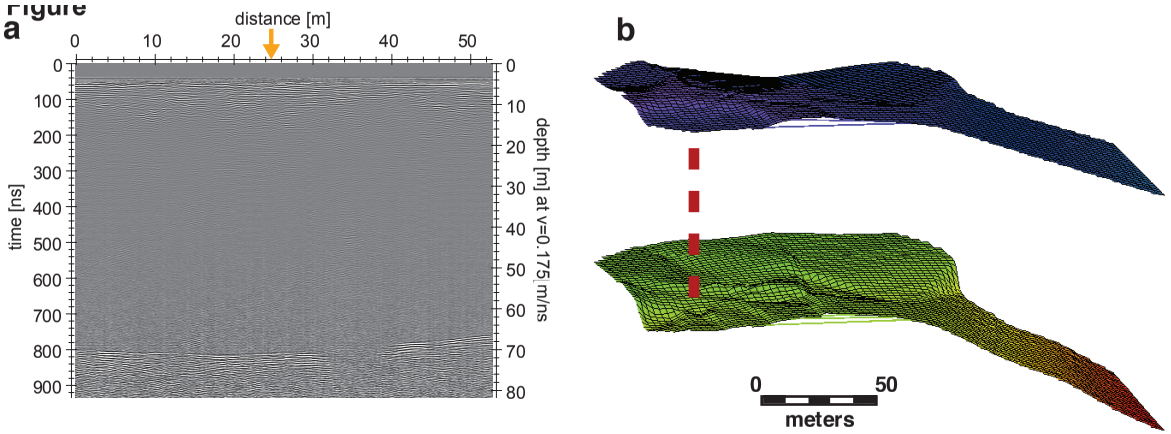
a
distance [m]
0
10
20
30
40
50
time [ns]
0
100
200
300
400
500
600
700
800
900
depth [m] at v=0.175 m/ns
0
10
20
30
40
50
60
70
80
b
0
50
meters

Figure

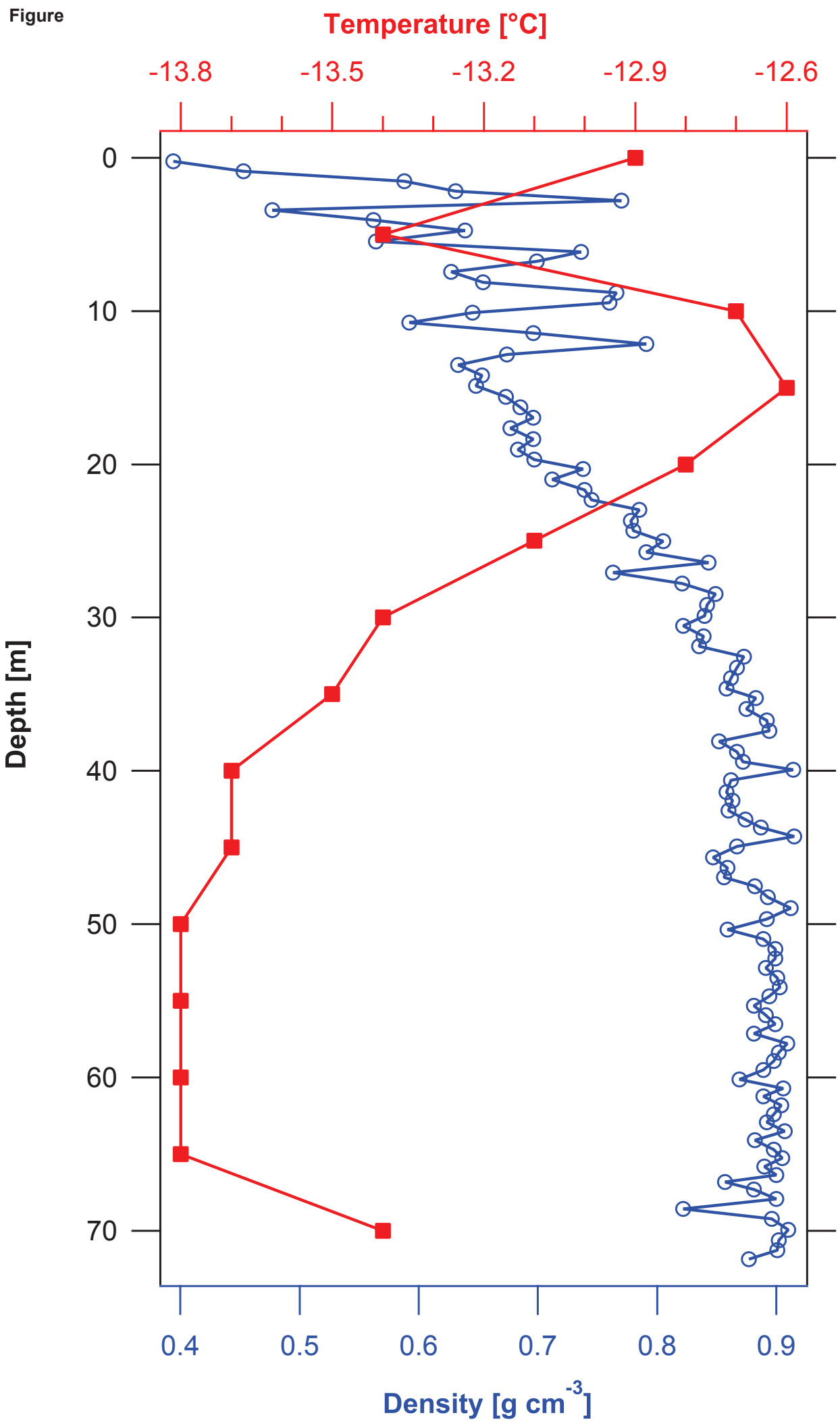
Temperature [°C]
-13.8
-13.5
-13.2
-12.9
-12.6
0
10
20
30
40
50
60
70
Depth [m]
0.4
0.5
0.6
0.7
0.8
0.9
Density [g cm-3]

Figure

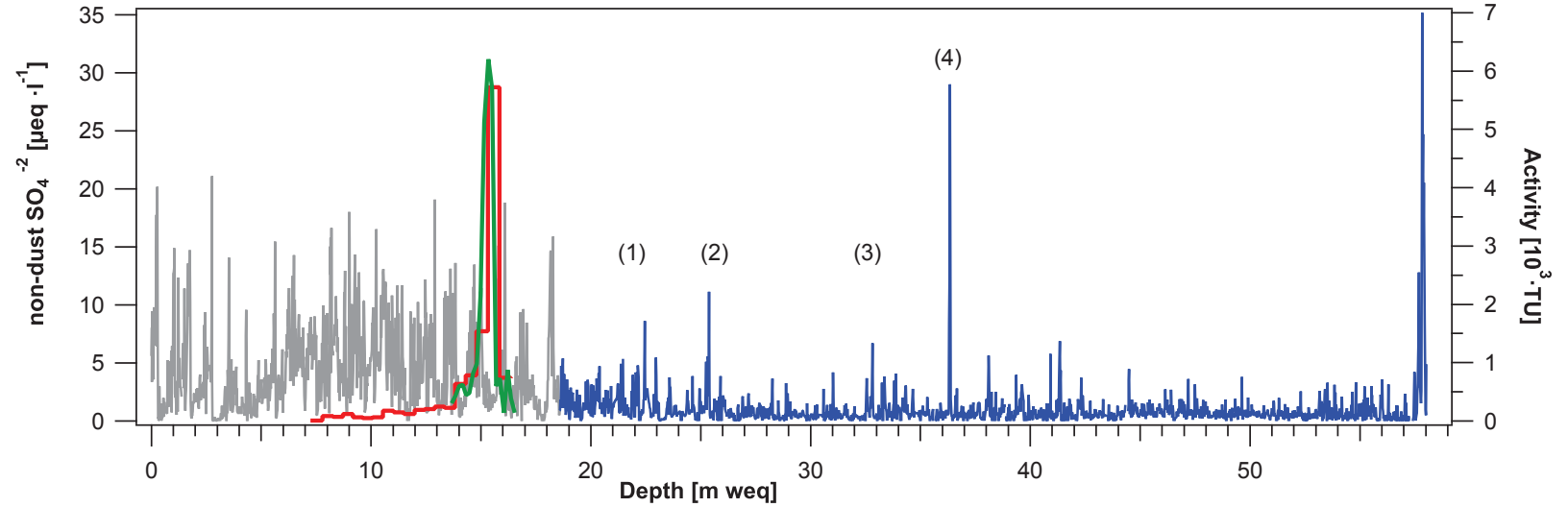
non-dust SO_4^{-2} [µeq ·l^{-1}]
Activity [10^3 ·TU]
Depth [m weq]
(1)
(2)
(3)
(4)
0
5
10
15
20
25
30
35
0
1
2
3
4
5
6
7
0
10
20
30
40
50

Figure

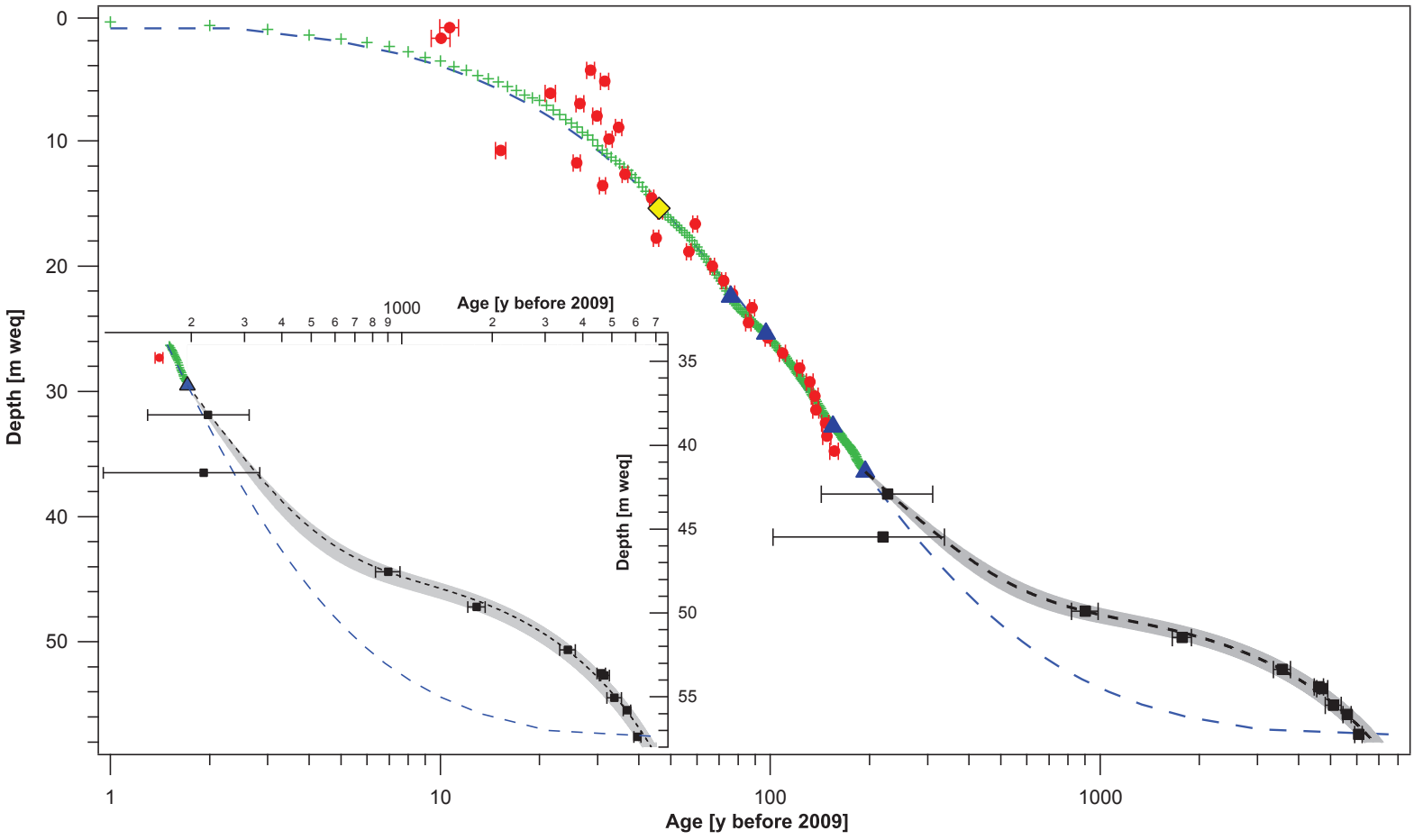
Depth [m weq]
0
10
20
30
40
50
1
10
100
1000
Age [y before 2009]
1000
Age [y before 2009]
Depth [m weq]
35
40
45
50
55

Figure

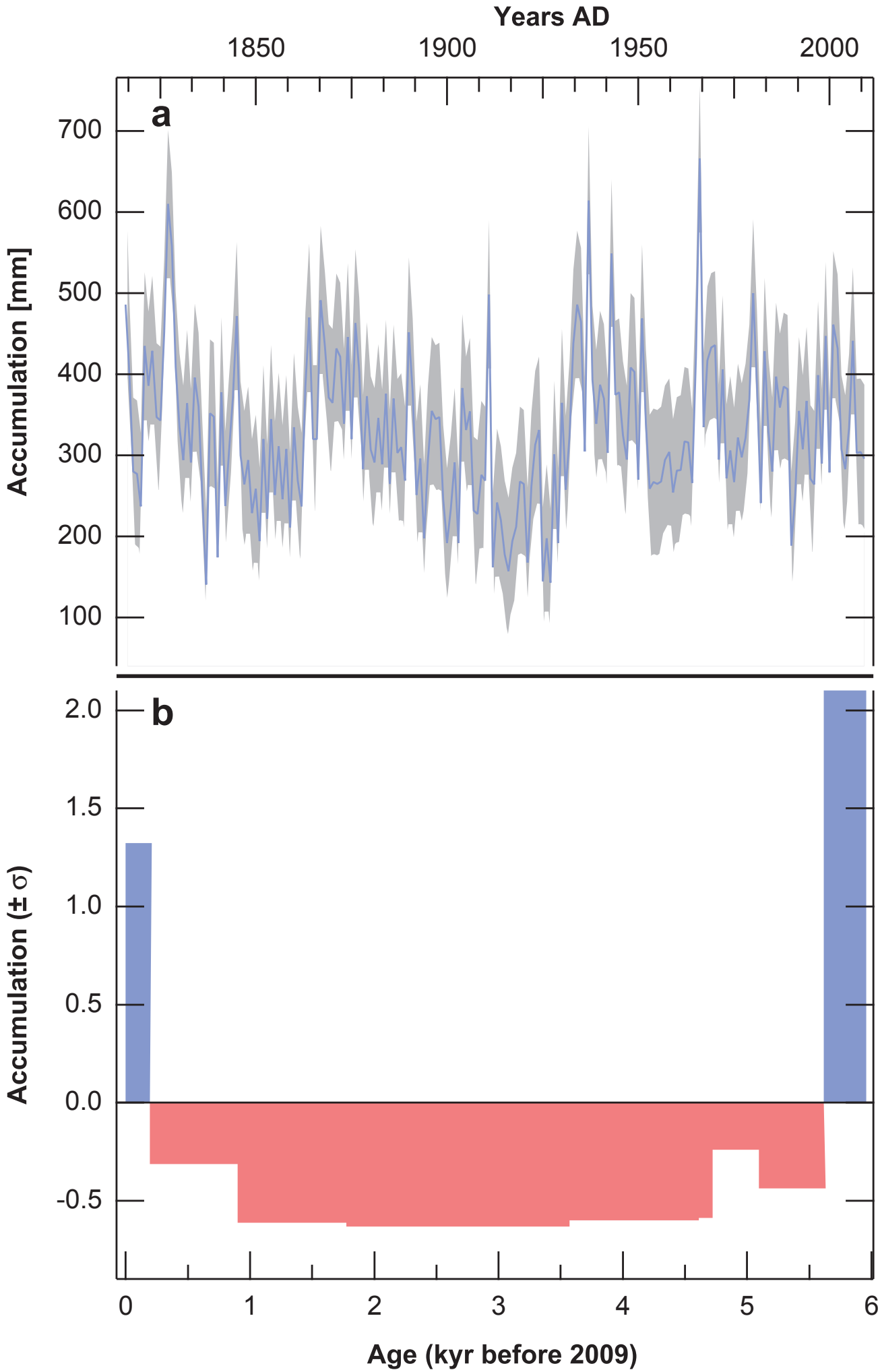
Years AD
1850
1900
1950
2000
a
700
600
500
400
300
200
100
Accumulation [mm]
b
2.0
1.5
1.0
0.5
0.0
-0.5
Accumulation (± σ)
0
1
2
3
4
5
6
Age (kyr before 2009)